LBL-34238
UC-410

Lawrence Berkeley Laboratory
UNIVERSITY OF CALIFORNIA

Accelerator & Fusion Research Division

Presented at the Accelerator Instrumentation Workshop, Berkeley, CA, October 27–30, 1992, and to be published in the Proceedings

Advanced Light Source Instrumentation Overview

C. H. Kim

October 1992

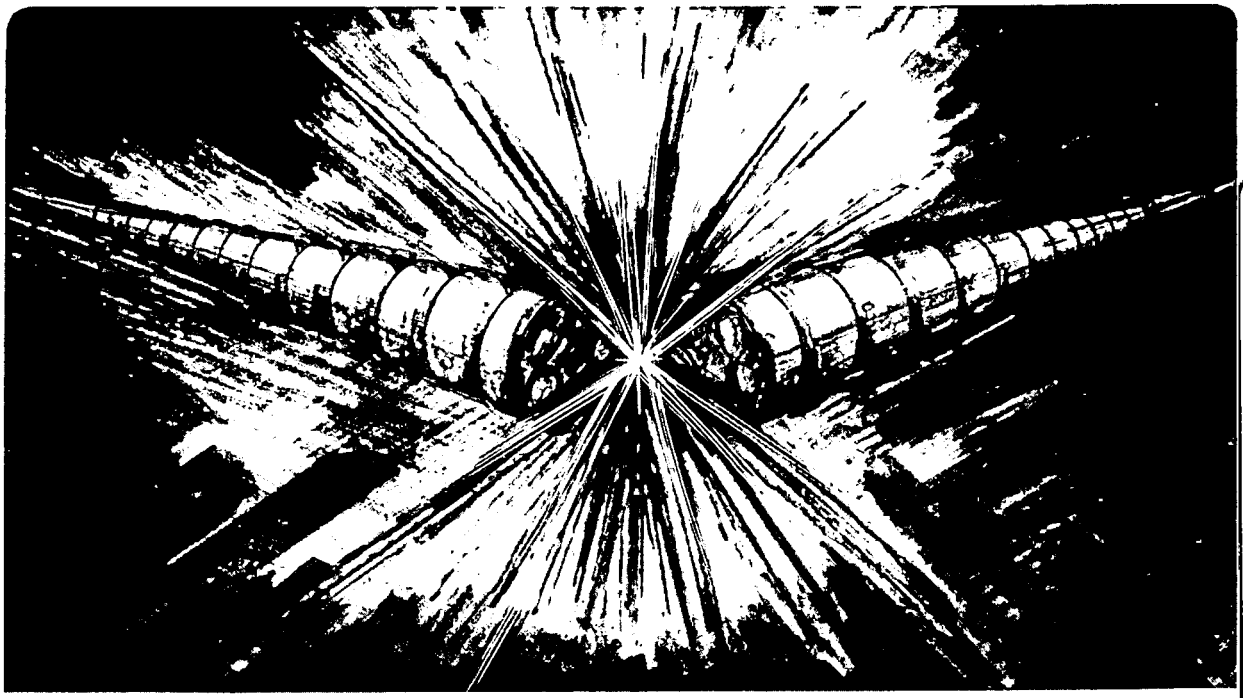

Prepared for the U.S. Department of Energy under Contract Number DE-AC03-76SF00098

DISCLAIMER

LBL-34238

ADVANCED LIGHT SOURCE INSTRUMENTATION OVERVIEW*

Charles H. Kim

Advanced Light Source
Accelerator and Fusion Research Division
Lawrence Berkeley Laboratory
University of California
Berkeley, CA 94720

October 1992

*This work was supported by the Director, Office of Energy Research, Office of Basic Energy Sciences, Materials Sciences Division of the U.S. Department of Energy, under Contract No. DE-AC03-76SF00098.

Advanced Light Source Instrumentation Overview

Charles H. Kim and James Hinkson
Lawrence Berkeley Laboratory, University of California, Berkeley California 94720

Abstracts

The accelerator instrumentation played a vital role in commissioning the ALS injector accelerator. It helped us to see whether electron dynamics agreed with our theoretical predictions and important beam parameters met the design specifications. It helped us to see where beam losses occurred and why. In this paper we will start with a brief description of the ALS accelerator complex and the expected performance of it. Then we will describe each diagnostics instrument by its construction, operational principle, requirements, and our experiences with it. We will describe the wall current monitor, the scintillator, the Faraday cup, the beam collimator, the beam position monitor, the direct-current current transformer (DCCT), the traveling wave electrodes (TWE), the Sabersky finger, and other special instruments. Finally, we will go into some detail on how we measured the beam emittances, the closed orbit, and the betatron tunes.

1. Introduction.

The Advanced Light Source [1], [2] is a dedicated state-of-the-art synchrotron radiation facility under construction at the Lawrence Berkeley Laboratory. It is expected to be operational in spring 1993 and serve the national user community with very bright photon beams in the spectral range covering from VUV to soft X-ray regime. The ALS accelerator complex consists of a 50 MeV linear accelerator (linac), a 1.5 GeV booster synchrotron and a 1 to 2 GeV storage ring. The storage ring is classified as a third generation synchrotron radiation source whereby the beam-optics design is optimized for very small beam sizes and long straight sections for the state-of-the-art insertion devices such as wigglers and undulators. Commissioning of the 198.6 meter long storage ring is expected to begin in January 1993.

The ALS injector [3], [4] is operational and meets its full design specifications at this time. The accelerator instrumentation played a vital role in commissioning the ALS injector in a timely progression. This paper is not intended to be a comprehensive review on accelerator instrumentation, but to describe specifically various diagnostic instruments that we used in commissioning the ALS injector. The ALS injector accelerator consists of the electron gun, the gun-to-linac (GTL) beam line, the linac, the linac-to-booster (LTB) beam transfer line, the booster synchrotron, and the booster-to-storage-ring (BTS) beam transfer line. The injector repetition rate is 1 Hz. Figure 1 schematically shows the layout of the accelerator complex.

The gun produces electron bunches in 8 nsec intervals with the number of bunches variable from 1 to more than 12. Each bunch has a pulse duration of about 1 nsec rms and contains up to 2.5 x 10^{10} electrons (4 nC). We use focusing coils and bunchers in the GTL beam line to compress each electron bunch transversely and longitudinally for efficient capture in the linac[5]. Good compression is also necessary to achieve a high beam quality in the linac with low beam emittances and low energy spread. Bunchers consists of a 125 MHz subharmonic buncher, a 500 MHz subharmonic buncher, and a 3 GHz traveling wave buncher. Timing of the bunches and the rf amplitudes and relative phases of the bunchers must be carefully adjusted. The linac proper consists of two two-meter, 3-GHz, disk-loaded waveguides. The accelerating waveguides have a constant-impedance structure for the $2\pi/3$ traveling wave mode. Every 24-th linac rf bucket is loaded with one electron bunch if the bunchers are tuned as designed.

The beam must be conditioned properly for the right beam size, energy dispersion, and injection angle in the LTB transfer line for efficient injection into the booster. The electrons are injected onto the booster axis and kicked into the orbit via a fast injection kicker magnet. The kicker magnet must

be completely turned off by the time the first injected bunch comes back to the injection point after making one turn around the booster. Timing of injection into the booster must be precise because it occurs as the booster dipole fields are ramped.

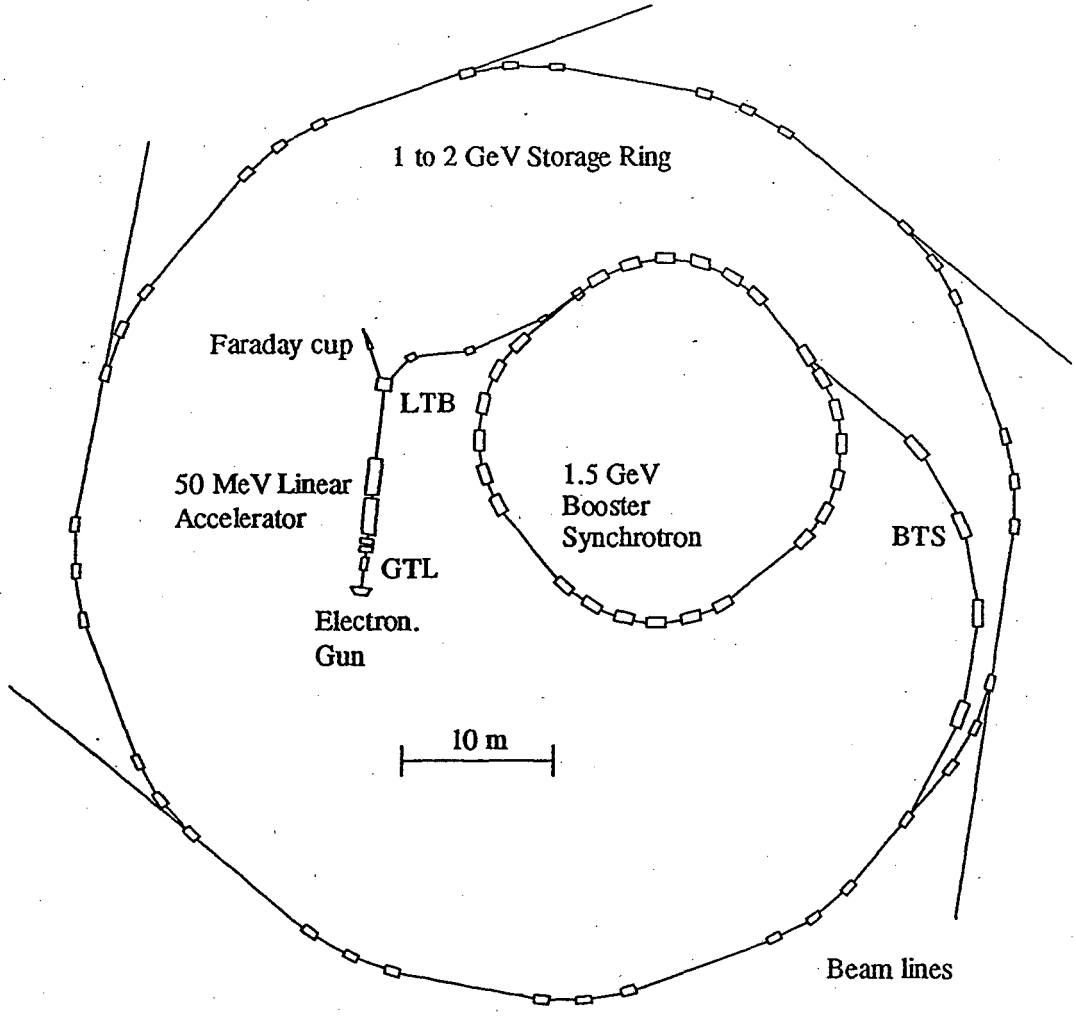

Figure 1. Advanced Light Source (ALS) accelerator layout

Acceleration to 1.5 GeV in the booster takes about 0.34 seconds. During acceleration, the quadrupole fields must be ramped at the same rate as the dipole fields so that the betatron tunes do not shift during acceleration. Booster rf fields must also ramp to keep proper bucket size and to compensate for energy loss due to synchrotron radiation at higher energies. The booster rf frequency is 500 MHz and the harmonic number 125. Every fourth rf bucket is filled for the duration of the injected bunches and the rest of the buckets are left empty for the necessary injection kicker magnet fall time and extraction kicker magnet rise time. One booster orbit takes 250 nsec. Beam intensity, betatron tunes, electron orbits, beam energy, etc., are monitored during ramping. When beam is accelerated to extraction energy, three extraction bump magnets are turned on which pushes the booster orbit slowly towards the extraction septum magnet. Then, we wait up to 82 msec for the correct storage ring rf bucket to line up with the booster rf bucket. We then fire the fast extraction

kicker magnet and two septum magnets. ALS accelerator design parameters are summarized in Table 1.

Table 1. ALS Accelerator design Parameters

	Linac	Booster	Storage Ring	Storage Ring
Mode	-	-	Single bunch	Multibunch
Energy (GeV)	0.05	0.05-1	1-2	1-2
RF Frequency (MHz)	2998	499.654	499.654	499.654
Harmonic Number	-	125	328	328
Bunch Spacing (ns)	8	8	-	2
Revolution Period (ns)	-	250	656	656
Repetition Rate (Hz)	1-10	1	-	-
Number of Bunches	1-20	1-12	1	<250
Charge (nC/bunch)	1	0.8	5	1
Average Current (mA)	125	3 - 20	7.6	400
Bunch Length (2s ps)	30	100		28-50
Tune ν_x, ν_y	-	5.80, 2.79		14.28, 8.18
Syn Freq (kHz)	-	256-44		14

The accelerator instrumentation played a vital role in commissioning and qualifying the ALS injector accelerator. It helped us see whether electron dynamics agreed with our theoretical predictions (model validation). It helped us verify accelerator parameters so that important beam parameters have met the design specifications (qualification). It helped us see where beam losses occurred and, in most cases, why (improve reliability). It will help operators tune the accelerator quickly and serve user's requirements (user friendliness) . ALS accelerator instrumentation is summarized in Table 2.

Table 2. Summary of ALS accelerator instrumentation.

	GTL	Linac	LTB	Booster	BTS	Storage ring
WCM	1	-	-	-	1	-
Faraday cup	-	-	1	-	-	-
DCCT	-	-	-	1	-	1
Scintillator	2	2	6	5	7	1
BPM (buttons)	2	1	-	32	-	96
BPM (TWE's)	-	1	7	3	6	-

We will begin with beam intensity monitors in the next three sections. Wall current monitors, a Faraday cup, and DCCT's are described. Detailed design and bench testing of the beam position monitors have been described previously by one of the authors[6]. They have four electrodes with their difference signals indicating beam positions. BPM sum signals provide relative beam intensity information which is useful for tuning the beam transfer line.

2. Wall Current Monitor

It indicates electron beam current by measuring the return current (image current)along the beam pipe. The return current produces voltage drop across resistance inserted in the pipe wall. Figure 2 shows wall current monitor components. The beam pipe is interrupted with a commercially available flanged ceramic tube. The ceramic on the vacuum side is plated with a thin layer of metal to prevent damage from sparks and to suppress cavity modes. The metal (about 60 Ω per square) shunts the resistors circling the ceramic on the outside. There are 20 high frequency ceramic resistors 39 Ω each. surrounding the ceramic, giving a total resistance of 2 Ω.

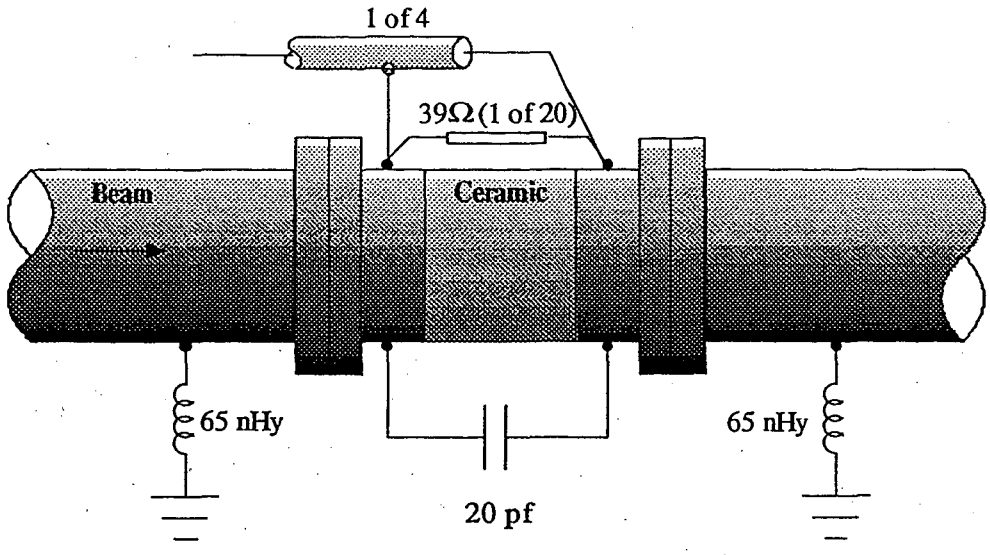

Figure 2. Wall current monitor components

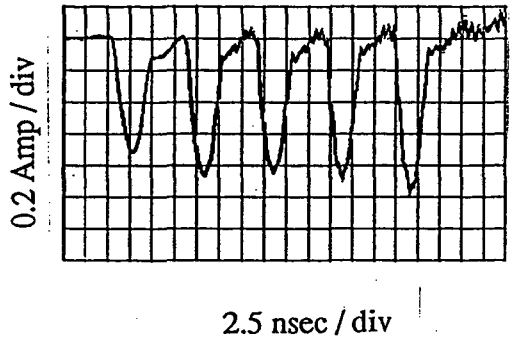

Figure 3. Wall current monitor signal

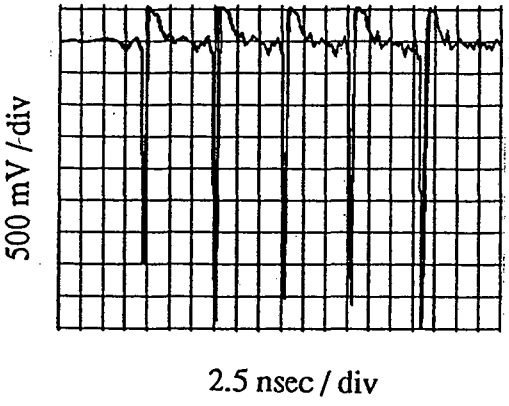

Figure 4. BPM sum signal at 25 MeV

The high frequency response of the wall current monitor is determined by the shunt capacitance (20 pf) across the ceramic gap, which forms a low pass filter, with the (-) 3 dB roll off at 4.2 GHz. The low frequency response is determined by the shunt inductance (65 nHy x 2) across the gap, which forms a high pass filter, with the (-) 3dB roll off at about 2.4 MHz

The sensitivity of the wall current monitor should be ideally 0.5 Amp/Volts. In order to reduce the signal dependence on beam position however, the beam signal is tapped off at four places equally spaced around the resistor belt and summed in hybrid power combiners. Frequency responses and attenuation factors of the hybrids and cables will alter the sensitivity. Bench calibration showed that the actual sensitivity is 0.4 A/V at the frequency range of the present interest.

Figure 3 shows a typical wall current monitor waveform measured 69 cm from the electron gun and shows the intensity and the time structure of the electron gun current.

The signal was digitized by the Tektronics 2440 oscilloscope and send to the control room via an optical cable. The electron gun has a triode geometry in which an rf voltage with a frequency of 125 MHz and an amplitude of 0-to-70 Volts is applied between the cathode and the grid. In practice the rf voltage is clipped with a dc bias of up to 30 V to make the pulse width shorter. Figure 4 shows a beam-position-monitor (BPM) raw sum signal at 25 MeV point in the linear accelerator. We used this signal to tune the bunching system, although the bandwidth of the scope was not wide enough to show the real pulse duration. Beam position monitors will be described in more detail in section 6.

3. Faraday Cup

We measure the temporal characteristics and the total charge of the beam with the Faraday cup. An ideal Faraday cup is a very large metallic box with a small hole through which charged particles enter. The box or the "cup" is connected to the ground via a characteristic resistor. The charged particles draw image charges on the metal surface via this resistor. The induced voltage across the

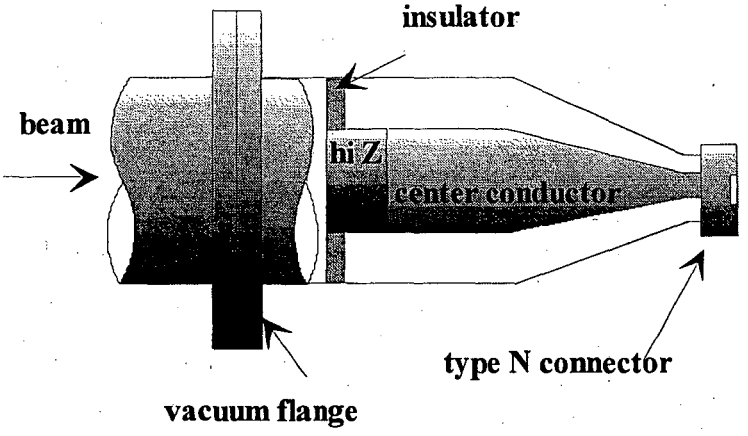

Figure 5. Schematic diagram of the Faraday cup

resistor is equal to the electron beam current. This picture suggests that a voltage change appears on the resistor when a particle enters the box. When it hits inside wall of the box it combines with the image charge and there is no net change of electrical charge on the box, thus no signal. Secondary charged particles generated at the impact however can give spurious signals when they leave the Faraday cup. For this reason Faraday cups must be made very deep and/or be biased positively to prevent this from happening.

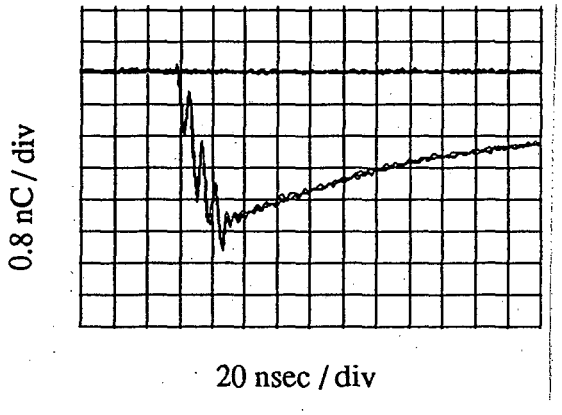

Figure 6. An integrated Faraday cup signal

Figure 5 shows the Faraday cup used on the 50 MeV diagnostics beam line. The high-Z material in the front of the center conductor stops electrons. The tapered coaxial geometry makes it useful for broad-band measurements. A high quality Heliax coaxial cable directs the cup signal to a transient digitizer having 5 GHz single-shot band-width.

The Faraday-cup rise time is about 200 psec. The Faraday cup was more useful for monitoring the total charge in the beam. Figure 6 shows an integrated Faraday cup signal with four bunches. One can count the number of bunches by counting the number of steps during integration.

4. Direct-Current Current Transformer

DC current transformer (DCCT) gives the most accurate method of measuring the DC component of a circulating beam in a circular accelerator. This is a parametric current transformer based on the principle of second harmonic generation. This principle is also used in the flux-gate magnetometer for measurement of Earth's magnetic field and transductors we use to regulate and measure magnet currents. Figure 7 shows a schematic diagram of a DCCT. The magnet core encircling the beam pipe couples to the DC and low frequency magnetic field of the beam. The ceramic gap in the beam pipe forces the low frequency wall currents to loop through the cores providing this coupling. Without the gap the low frequency fields would penetrate the beam pipe and couple to the core but so would other currents following along the beam pipe. Those foreign currents can be greater than the beam current. The high frequency components of the beam are shunted past the cores by the gap capacitance.

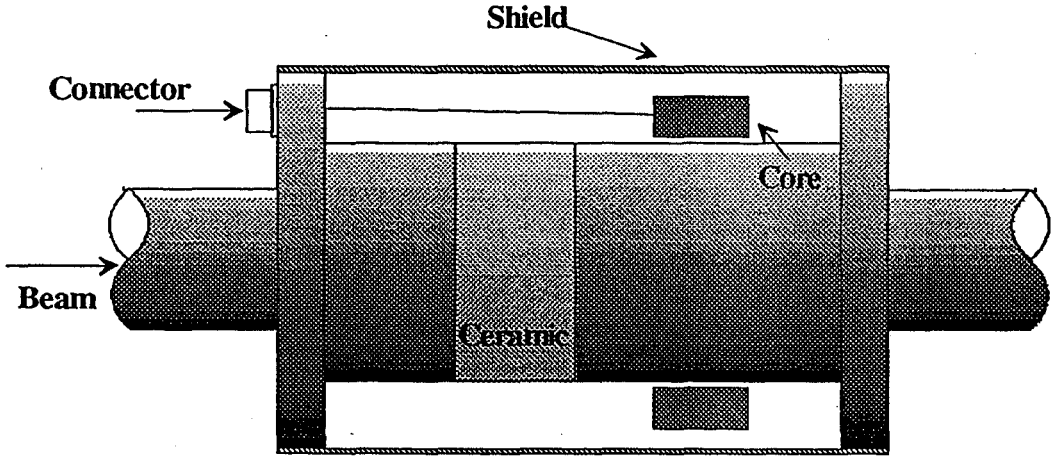

Figure 7. DCCT

The DC fields are measured in the following way: the core is driven into positive and negative saturation at 55 Hz by a current square wave from the processing electronics. A sense winding on the core couples to the drive winding and picks up a 55 Hz signal with an average value of zero. The symmetry of the B-H curve insures that the sense winding signal has only the odd harmonics of 55 Hz if there is no beam. When a foreign DC current (the beam) is present in the pipe the average is no longer zero. The B-H loop of the core is skewed somewhat now by the DC and low frequency of the beam magnetic field. A second harmonic voltage, 110 Hz, is created by the asymmetry of the B-H loop and is picked up by the sense winding. A synchronous detector samples the 110 Hz signal and creates a DC feedback current which drives a third winding, canceling the original offsetting flux. The ampere-turns of the feedback circuit exactly match and cancel the ampere-turns of the beam thus restoring the B-H loop symmetry. This feedback current is measured and becomes a DC voltage proportional to beam current. The cores are made of annealed high-permeability material. Strong external magnetic fields or mechanical shock can damage the cores. The shield covering the DCCT is necessary to shunt foreign currents and to keep high frequency rf from radiating. The structure resonates at 40 MHz, the 10th harmonic of the beam revolution frequency. It is important to keep the covers in place.

Figure 8 shows a typical booster DCCT waveform. The injected beam had 4 bunches over 24 ns with beam loading compensation in the linac. More than 90 % of the injected beam was captured to 12 mA booster current accelerated all the way to full energy and extracted. The electronics are very sensitive to rf interference and the magnetic modulation at 55 Hz somehow entered as a 55 Hz ripple on the waveform.

The storage ring DCCT will perform much better than the booster DCCT. Table 3 shows comparisons of some of the specifications for the two DCCT's. The storage ring DCCT will be connected to the control system via an intelligent local control (ILC). We will be able to take accurate readings of average current in the ring and observe the waveform on a scope. This device will have a di/dt output which will be a useful tuning aid when we try to maximize beam life time in the storage ring.

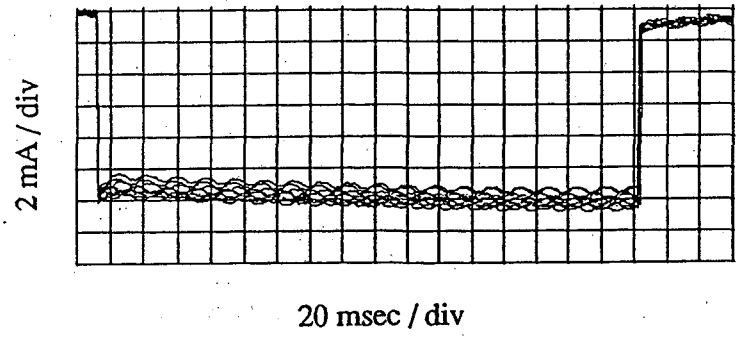

Figure 8. A typical booster DCCT wave form showing 12 mA beam accelerated to full energy in 350 msec.

Table 3. Comparison of some of the specifications of the booster and the storage ring DCCT's.

Specifications	Booster	Storage Ring
Range (mA)	100	10 (or 1000)
Full Scale Output (V)	10	10
Frequency Response (kHz)	0 - 1	0 - 20
Accuracy (%)	1	+- 0.1
Slew Rate (V / μs)	-	0.1
Resolution (μA)	100	5

The storage ring DCCT is very sensitive to stray magnetic fields. We will install a magnetic shield which should prevent the nearby steering magnet from causing DCCT errors. Each time the DCCT is energized, it is degaussed. The ceramic gap contributes to the vacuum chamber impedance and therefore, beam instabilities. The shield will probably resonate with certain beam harmonics and create an objectionable narrow band beam impedance. To be UHV compatible the shield is designed to be bakable. Thermocouples to monitor the bake temperature and a water cooling to protect the core from overheating are added.

5. Scintillator

Scintillators generate a flash of light when high energy particles impinge upon them. A plate made out of or coated with scintillating material is placed in the beam path to measure beam positions and charge distributions. Because of its simplicity and visual effects scintillators are very popular among accelerator operators. Various users call it by other names such as a target, a flag, a

fluorescent screen, a paddle, etc. Scintillators have some disadvantages. For example, simultaneous monitoring at different locations and dynamic feedback are impossible because of destructiveness and slow electronic data processing. However, recent advances in charge-coupled-devices and image processing technologies make scintillators more useful for other applications. We used scintillators for beam steering, beam envelope matching, magnet strength calibration, emittance measurement, etc. One of the scintillators that is located in the dispersive region of the LTB line showed some aspects of the beam time structure which were used for tuning the bunchers.

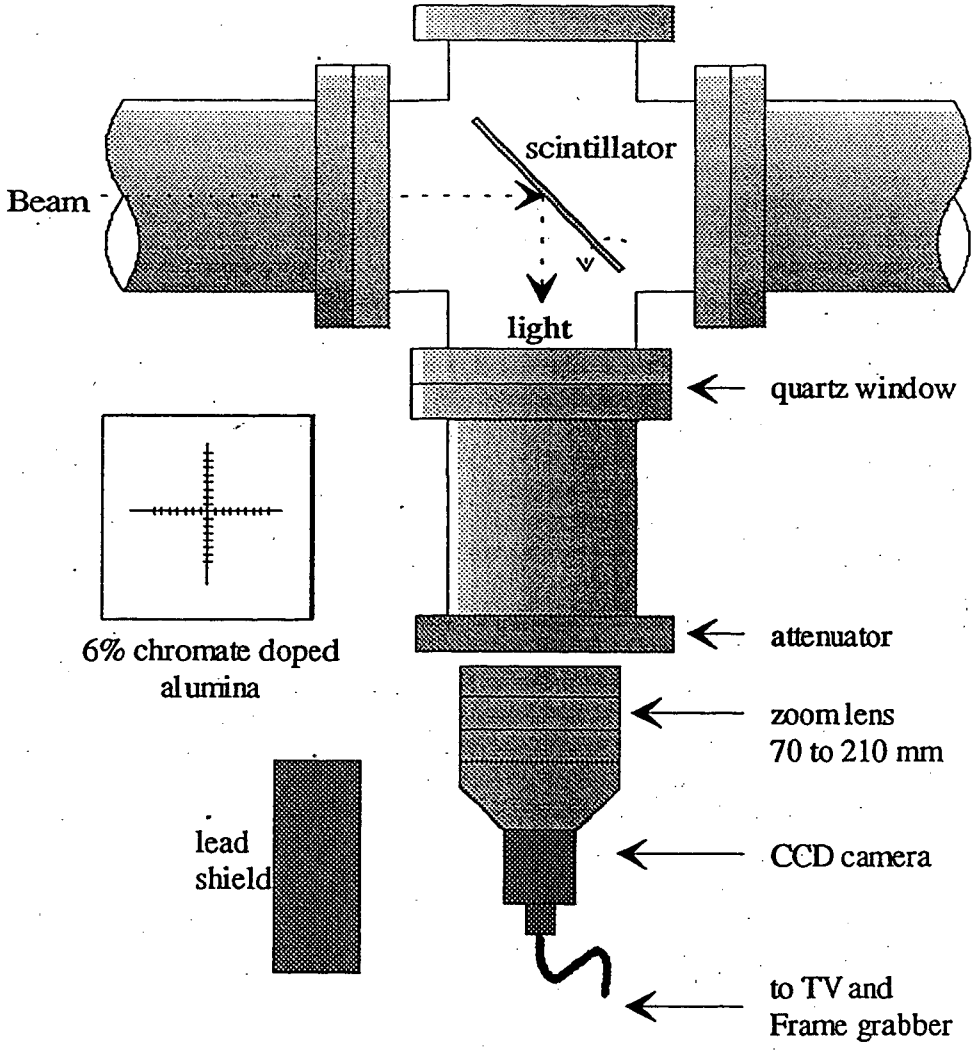

Figure 9. A scintillator-TV monitor station

5.1 Description

Figure 9 shows a typical scintillator-TV monitor station configuration. The scintillating material is chosen according to one's requirements for the sensitivity, dynamic range, time response, resistance to radiation damage, linearity with beam intensity, vacuum compatibility, etc. We used 6 % chromate doped alumina (Chromox 6 manufactured by Morgan Matroc Limited in the UK) for beam energies above 25 MeV. Dimensions before cutting are 75 mm x 75 mm x 1 mm. For beam intensities of about 1 nC per bunch at this energy charge accumulation was not a problem. Recent test showed that

the Chromox 6 scintillators produce copious infra-red and have a long after glow. After glow was not a problem for our time-integrating applications. We had been using Zinc Oxide coated stainless steel plates in GTL. We later tried Chromox 6 as they become available in GTL but charge accumulation on the scintillator surface was a serious problem. We think that higher electron current and low electron energy had contributed to the problem. Other users incorporate some kind of discharge routes (such as metal coating or fine wire mesh) to solve the charge accumulation problem.

We are currently using 70 - 210 mm, f5.6 zoom lenses for imaging. We chose zoom lenses because they simplify optical setups. Large distance from the source and small lens aperture in this design do not have high light gathering power but enough intensity for most of our applications. The zoom lenses are not radiation resistant and will probably brown from radiation damage in time. They can be made clear again by exposing them to UV radiation. The zoom lens is mounted on a CCD camera (we used Fairchild Weston CCD5000 camera system). The CCD image sensors have 483 x 378 pixels. The horizontal resolution of the camera is 483 TV lines. CCD response peaks between 700 and 900 nm. The TV signal is then sent to the control room for image monitoring or image processing and digitizing. We used Data Translation's frame grabber model DT5661.

5.2 Magnet calibration and tuning

The most frequent and common usage of scintillators is to make quick visual observations of the beam image. A gross deformation and/or loss of symmetry in the beam image indicate that beam is mis-steered and perhaps scraping the wall. Halo formation usually indicates that the focusing is too strong and the beam envelope is not very well matched. This technique is useful for beam steering and focusing in the linac and in the LTB line.

We also used the scintillators effectively for tuning the bunching system in the GTL line. We monitored the beam size and shape in the LTB line just after the first bending magnet where energy dispersion is large. If the bunching system is not tuned well energy spread is large and the beam size is large at this point. If bunching is good we can see well-separated individual microbunches on the screen.

Scintillators were used for calibrating quadrupole magnets. A steering magnet located upstream and one or two scintillators located downstream of the quadrupole are sufficient.

For calibrating dipoles one scintillator downstream is sufficient for a relative measurement. For example, we measured the flatness of the booster injection kicker magnet using this configuration. We measured the beam position as a function of the magnet turn-on time and verified that indeed we have a 100 nsec flat-top within ±0.5 %. For an absolute dipole strength measurements two scintillators upstream and two scintillators downstream are required. Scintillators are more accurate than beam position monitors but are destructive of beam and more expensive.

5.3 Emittance measurements

ALS beam emittances were measured at three accelerator locations: at the exits of the gun; at the linac exit; and at the booster exit. A pepper-pot apparatus was used at the gun exit. Beam was let through a collimator which had an array of small holes. This method is good in the GTL line where the coulomb repulsive forces (space charge forces) dominate beam optics. We measured beam emittance there by measuring the divergence of the little beamlets using a scintillator. The collimator hole size, the hole separation, and the drift distance between the collimator and the scintillator were optimized for the expected beam emittance so that the beamlet images do not overlap and yet obtain the best accuracy.

Beam emittances at booster exit were measured by just measuring the horizontal (i = x) and the vertical (i = y) beam sizes (x_i). Calculated values for β functions and the relationships, $x_i = \sqrt{(e\beta_i)}$ were used to calculate beam emittances.

Beam emittances at the linac exit were measured using two scintillators and a quadrupole triplet. The first scintillator screen is located at location "1" upstream of the triplet. The other screen is at

location "2" downstream of the triplet. The beam emittance (ε) and the Twiss parameters (α_i, β_i, γ_i) at these locations are related as in the following equations:

$$\beta_1\gamma_1 - \alpha_1^2 = 1 \tag{1}$$

$$\beta_2\gamma_2 - \alpha_2^2 = 1 \tag{2}$$

$$\begin{pmatrix} \alpha 1 \\ \beta_1 \\ \gamma_1 \end{pmatrix} = \begin{pmatrix} n11 & n11 & n11 \\ n11 & n11 & n11 \\ n11 & n11 & n11 \end{pmatrix} \begin{pmatrix} \alpha 2 \\ \beta_2 \\ \gamma_2 \end{pmatrix} \tag{3}$$

$$\sigma_1 = \sqrt{\varepsilon \beta_1} \tag{4}$$

$$\sigma_2 = \sqrt{\varepsilon \beta_2} \tag{5}$$

We can calculate the matrix elements n_{ij} using the magnet-measurement data, and measure beam sizes at both locations. We can then solve 7 coupled equations with 7 unknowns (beam emittance, and the Twiss parameters). The presence of the triplet is not necessary, but increases the accuracy of the emittance measurement. A beam size measurement at location "1" in the horizontal plane is shown in figure 10(a). Beam profile was integrated in the vertical direction. The image without the beam were subtracted from the image with the beam to reduce the background noise. Horizontal beam sizes at location "2" for several triplet settings are summarized in figure 10 (b).

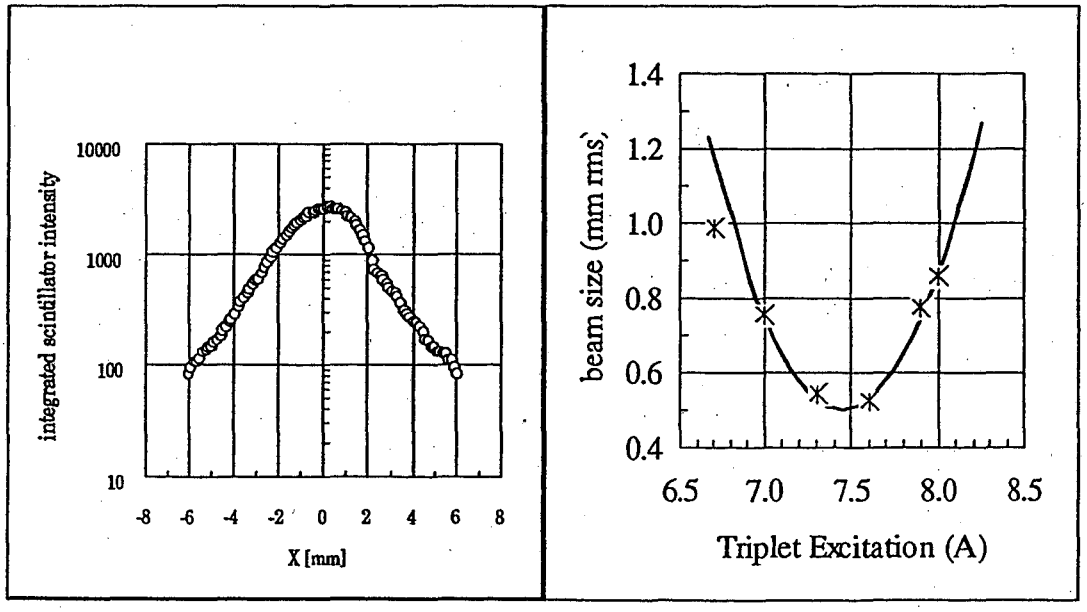

(a) (b)

Figure 10. Measured horizontal beam profile at location 1 (a) and location 2 (b). Data points in figure (a) are one pixel apart.

Emittance measurements and information on the Twiss parameters are essential in developing a model for the LTB beam transfer line. Accuracy of the emittance measurement and the model accuracy depends critically on the accuracy of the magnet strength measurements. The results of our measurement will be published elsewhere.

6. Beam Position Monitors

Because of their non-destructiveness for the beam and fast speed with which data can be processed, various types of beam position monitors are extensively used throughout the ALS accelerator system. Fast and simultaneous measurements of the beam positions and the relative intensities at different locations in the accelerator are very important for tuning and feedback stabilizing of accelerators. BPM's were used for tuning the beam transfer lines, injection and first- turn studies in the booster synchrotron and the storage ring, tune measurements, closed orbit measurement and correction, feedback stabilization, etc. A BPM system consists of an array of beam pickup electrodes, a set of high-quality coaxial cables, a bin of processing electronics, and a controlling computer. Careful preparations of the hardware, software, and testing of them were necessary for each of these applications.

One of us (JH) presented a detailed description of engineering, fabrication, bench testing, engineering problems, and solutions of beam position monitors at the CEBAF accelerator instrumentation work shop in 1991.[6] In this section we will briefly review the basic principles and our operating experiences of the beam position monitors during commissioning of the ALS injector.

6.1 Requirements

The storage ring BPMs are required to make continuous, non-destructive measurements of average beam position all the time, and deliver data to the orbit-control computer at 10 Hz. In addition, single-turn position data is to be accumulated at the ring revolution frequency and stored in internal BPM memory.

The booster ring BPMs function similarly to those in the storage ring with the performance specification being less rigorous. The booster ring BPMs report an average beam position at a selected time in the booster energy ramp (0-0.34s) at 1Hz. Single turn measurements are made also. The booster ring revolution frequency is higher, 4MHz, making single turn measurement timing a little more difficult.

BPMs in the Linac and beam transport lines measure beam at 1 to 10 Hz. There are 17 BPMs located in these areas. The beam repetition rate is low here, so we have slightly modified the storage ring BPM design to accommodate this lower rate. Table 4 shows the basic specifications for the BPMs in the different accelerator areas.

Table 4. BPM Electronics Specifications:

Parameter		Storage Ring	Booster	Linac, LTB, BTS
Resolutions (mm)	(low speed)	0.01	0.1	0.1
	(high speed)	0.5	0.5	-
Repeatability (mm)	(low speed)	0.03	0.1	0.5
	(high speed)	0.5	1.0	-
Data Storage (turns)		1023	1023	-
Response	(low speed, Hz)	20	1	1
	(High Speed, MHz)	5	7	-
Dynamic Range		40	40	50
Center Frequency (MHz)		500	500	500
Beam Pickup Style		Button	Button	Button and Stripline
Pickup Coupling (ohm @ 500MHz)		0.1	1.0	1.0 and 8.0

6.2 Mechanical and electrical properties

The ALS storage ring vacuum chambers are formed by two machined pieces of aluminum which are welded together. Very intricate machining was performed on the top and bottom of the slabs to accommodate magnet pole tips, flanges, diagnostic ports, BPM pickups, photon stops, vacuum pumps, and the electron beam channel. We use button style electrodes for BPM pickups in the storage ring as shown in figure 11, because they produce lower beam impedance and allow precision alignment. A button pickup is usually a thin, circular metal disk supported by the center conductor of a coaxial vacuum feed-through. The button is mounted flush with the wall of the beam vacuum chamber to avoid being struck by the beam. Where synchrotron radiation is present the buttons are configured to avoid being struck by the radiation, or a mask is installed to intercept the radiation. Button diameter is equal to twice the rms beam bunch length in order to collect maximum charge and to have good position sensitivity.

The booster BPM system is not required to perform as accurately as the storage ring system because of the large dynamic aperture. There is one BPM near each of the 32 quadrupoles. Each array, is composed of four button style pickups rotated 45 degrees from the horizontal plane, as shown in figure 12.

In the Gun-to-Linac (GTL) section where longitudinal space is limited we installed the CERN LEP button. The remainder of the BPM pickups in the transfer lines are striplines. Figure 13 shows the layout. These striplines are 150 mm long and have a 1 / 4 resonance at 500 MHz. This length was chosen to provide resonant drive for the 500 MHz bandpass filters in the detector electronics RF input section. All symmetrical striplines produce an inverted echo pulse (bunch length << stripline length) at a time 2l / c. With a length (l) of 150 mm, our stripline echo pulse occurs 1 ns after the prompt pulse providing resonant excitation for the filter. The coaxial feedthroughs we used for the striplines are type N, constant impedance devices from Cermaseal. They have good performance to about 3 GHz. We observe ringing at 5 GHz in the stripline signal when it is excited by the short linac beam pulse.

The electrical properties of these beam position monitors are summarized in table 5. The coupling impedance Z_i is defined as $V_i = Z_i I_b$ where V_i is the induced voltage on the i-th electrode and I_b is the beam current.

Table 5. The coupling impedance (Z_b @ 500 MHz), the capacitance, the self impedance (Z_S), and the sensitivity of pickup electrodes.

Pickup	Z_b (Ω)	C (pf)	Z_s (Ω)	S * (%/mm)
GTL and LN buttons	1	7	Reactive	6.0
LTB & BTS Striplines	8	NA	50	6.8
Booster Buttons	1.5	22	Reactive	4.4
Storage Ring Buttons (x)	0.1	25	Reactive	7.67
Storage Ring Buttons (y)	0.1	25	Reactive	5.72

* See equation (6) for the definition. The sensitivity figures apply only to a well centered beam.

The horizontal beam position as measured by two horizontally opposed pickup electrodes is calculated as follows:

$$X = (V_1 - V_2) / (V_1 + V_2) / S_x \qquad (6)$$

If the pickup electrodes are positioned 45 degrees from the measurement axes as in figure 11 for the storage ring or as in figure 12 for the booster the horizontal and vertical beam positions are calculated as follows:

$$X = [(Va+Vd)-(Vb+Vc)] / (Va+Vb+Vc+Vd+V)/Sx \qquad (7)$$

$$X = [(Va+Vb)-(Vc+Vd)] / (Va+Vb+Vc+Vd+V)/Sy \qquad (8)$$

where V_a, V_b, V_c, and V_d are detected button signals and S_i are the sensitivities.

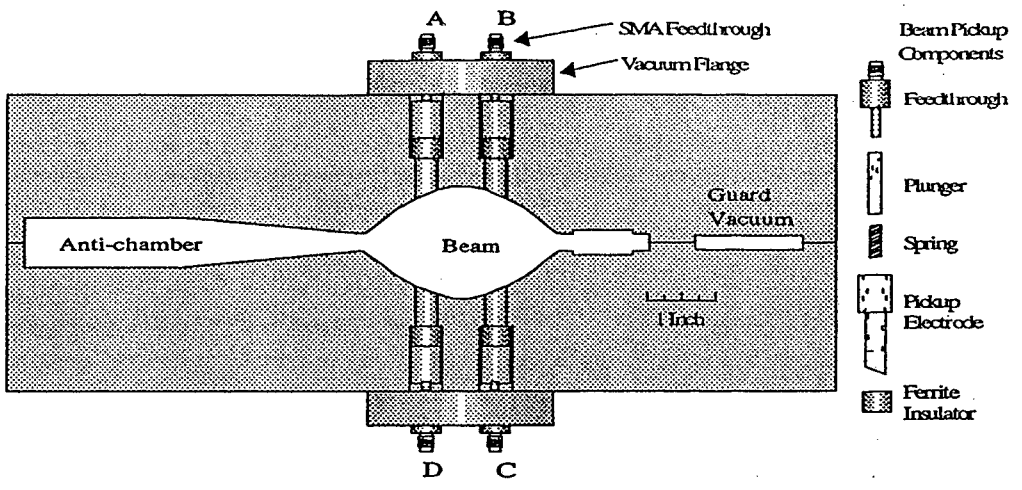

Figure 11. Cross section of ALS storage ring BPM buttons with exploded view of button parts parts.Shaded area is a very simplified representation of vacuum chamber.

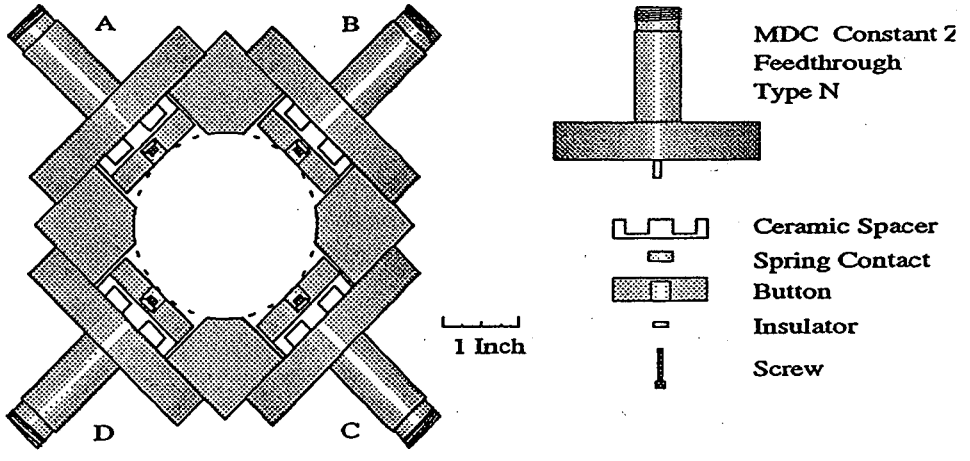

Figure 12. Booster BPM button arrangement.

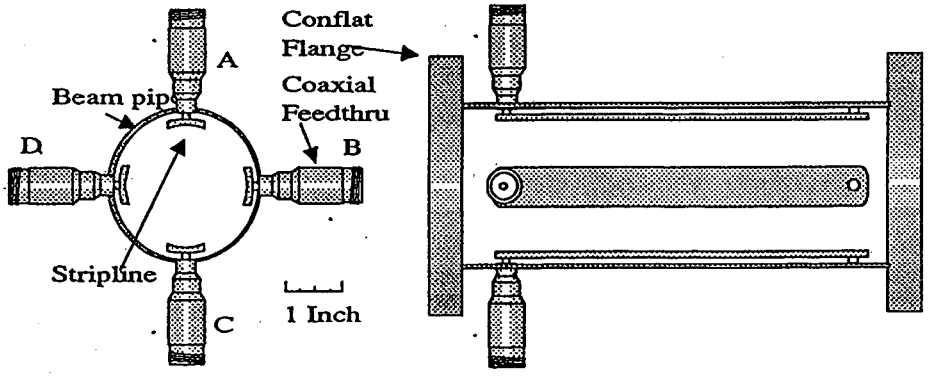

Fig. 13. Beam transfer line BPM striplines.

The sensitivities listed in table 4 are only for the well centered beams. A geometric non-linearity commonly known as the "pin-cushion" non-linearity produces errors at larger displacements. The linear position calculation at 20 mm was off by more than 5 mm for the storage ring BPMs. In order to make accurate position measurements at large displacements we make use of the method developed by Halbach.[7]

Errors due to mechanical offsets, unequal button capacitance, connector insertion loss, coaxial cable attenuation are mostly linear errors. They were compensated by measuring the button-to-button transfer function at our operating frequency, 500 MHz. Non-linear errors such as unequal saturation of amplifier gains in signal processing channels can lead to a very erroneous position readings.

6.3 Signal Processing

The block diagram in figure 14 illustrates the basic design for BPM signal processing. Each BPM bin contains four super-heterodyne, amplitude-modulation receivers tuned for 500 MHz. Beam signals from four pickup electrodes are band-limited by the coaxial cables and bandpass filters. This frequency is adequate to handle for arbitrary beam bunch-fill patterns in the storage ring. The frequency is also high enough for the pickup sensitivity (>200 MHz) and low enough to be under the cutoff frequency of the vacuum chamber (< 4 GHz) for signal isolation. Special precautions were taken in designing the BPM bin to insure that signal isolation between channels is greater than 60 dB at the operating frequency. [6]

The function of the RF converter module is to heterodyne 500 MHz beam signals down to 50 MHz and to inject calibration signals during the self-calibration sequence. There is no signal amplification in this module. The 500 MHz bandpass filter in the RF converter is an important component in the BPM electronics. We use tubular, 3-section, Chebychevs. They have excellent high frequency rejection and predicable pulse response. We found good agreement between SPICE evaluation of a 3-section, Chebychev bandpass filter at 500 MHz and a real filter. Figure 15 shows frequency and impulse response of the SPICE filter. The bandpass filter 3 dB-bandwidth is 25 MHz, much larger than required for single-turn position measurements in either the storage ring or booster. We could have tailored bandpass filter specifications to each application but determined it was less costly to customize the IF amplifiers. All of the RF modules are the same and will function in any of our applications.

The RF module mixer output contains not only our 50 MHz beam signal, but many other mixer products. The IF module input filter passes the 50 MHz signals and terminates the out-of-band signals in 50 ohms. This particular IF bandpass filter from MCL makes mixer IF signal processing quite simple. The monolithic integrated circuit (LM1211) from National Semiconductor is a broadband demodulator system originally developed as a receiver for local area networks. It operates between 20 and 80 MHz and has over 40 dB IF gain-control range (AGC).

The LM1211 detector operates with either AM or FM signals. For beam position monitoring we are interested in the amplitude of the 50 MHz IF signal, so we configured the detector as a quasi-synchronous, amplitude-modulation detector. By quasi-synchronous we mean that the internal phase detector is fed a reference signal developed from the IF signal itself. This of course means that no reference signal is available without an IF signal. A truly synchronous detector would have an unchanging reference signal of the proper frequency and correct phase. A limitation of quasi-synchronous detection is found when the internally-developed reference signal is no longer constant in phase and amplitude. This occurs when the IF signal is too low to saturate the output of the reference signal limiting amplifier. As a result we find a threshold below which the detector output is no longer useful. When this condition occurs, we increase the gain of the IF amplifier via AGC and restore good detector operation. At maximum gain the detector output is quite noisy, and much signal averaging is required in the ILC. [8] At high signal levels we find some gain compression in the IF amplifier output and also some compression in the detector output as it approaches 3.5V.

The signal appearing at the Video Out pin on the LM1211 is a pulse, 0 to +3V, having the shape of the beam bunch pattern (within bandwidth limitations). A single beam bunch generates a waveform similar to Figure 15 (right) at the output of the RF module bandpass filter. After mixing and filtering, this burst of RF is amplified and detected by the LM1211. The detected pulse duration

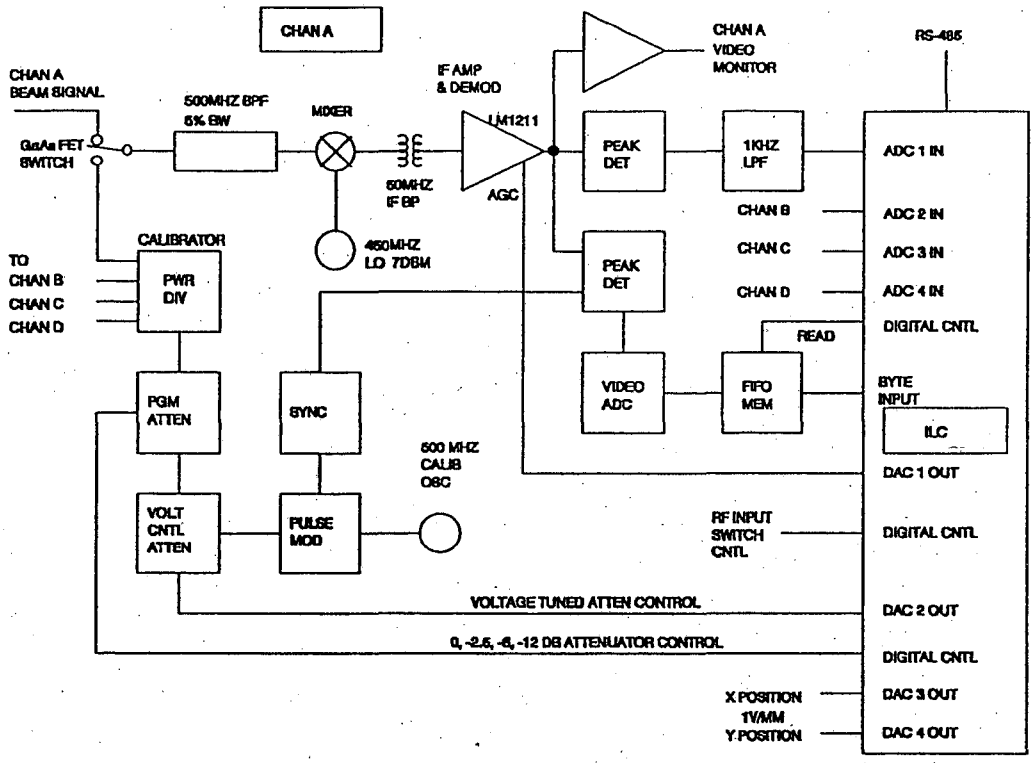

Figure 14. Block diagram of a BPM receiver. Only one channel is shown.

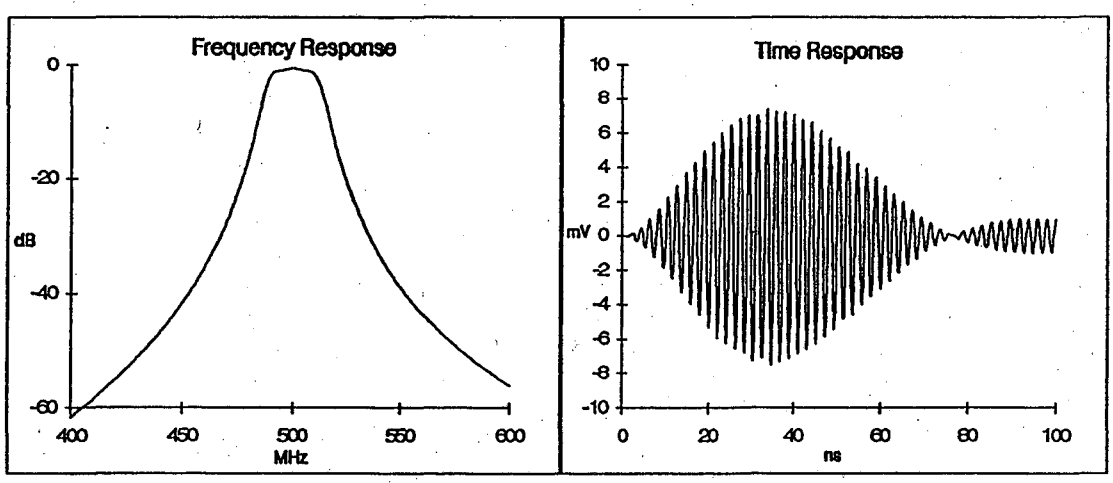

Figure 15. RF module input bandpass filter response. Impulse - 100ps, 1V pulse.

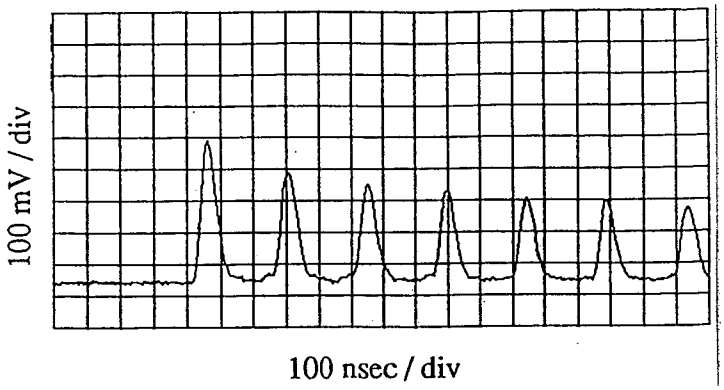

Figure 16. Booster BPM video signal. Sum of four channels.

is determined by the bandwidth of the IF amplifier, and for a single bunch is about 150ns. When the beam bunch pattern contains many contiguous bunches, the tuned circuits reach steady-state performance and the pulse appearing at the Video Out pin has the general shape and duration of the beam bunch pattern.

The LM1211 has good carrier suppression at the video output so no additional filtering IF is required. The video output pulses are directed in three paths. A unity-gain buffer amplifier delivers the pulses to a monitor jack on the rear of the BPM bin. The pulse amplitude is halved because of the amplifier's output impedance and cable impedance matching resistor. We use this pulse (and those from the other three IF amplifiers) for oscilloscope monitoring of BPM performance. A typical booster BPM video signal is displayed in figure 16. The first and the last BPMs in each of the 4 booster sectors are configured for an instant display of their video signals in the control room. This type of signal shows beam loss information in circular accelerators. Beam loss information in circular accelerators during the first few turns was especially useful for commissioning the booster.

In the second signal path the signal was passed to the buffer amplifier and to a peak-detector. From this point on the transfer line BPMs and circular accelerator BPMs are treated differently. When the BPM is monitoring low repetition rate beam (in the linac or in the transfer lines for example) the sample-and-hold (S-H) circuit following the peak detector is used to capture the voltage peak. In this case the active low-pass filter following the S-H is simply used as a DC amplifier to scale voltages for the analog-to-digital converter (ADC) in the intelligent local control (ILC).[8] Equations (6) through (8) and values in table 5 are used to calculate the beam positions and the results are displayed on the control-computer screen. A typical beam position measurements from the gun to the booster injection magnet is shown in figure 17. These BPM data agrees with the scintillator data to within 1 mm provided that beam is reasonably centered, electrons are not striking the electrodes, and the IF gain is set such that the video output is less than approximately 1 V. Figure 17 shows that beam is not aligned well in the GTL line. LTB BPM4 read about -4 mm when scintillator showed beam was centered. The cause of this discrepancy is unknown at this time.

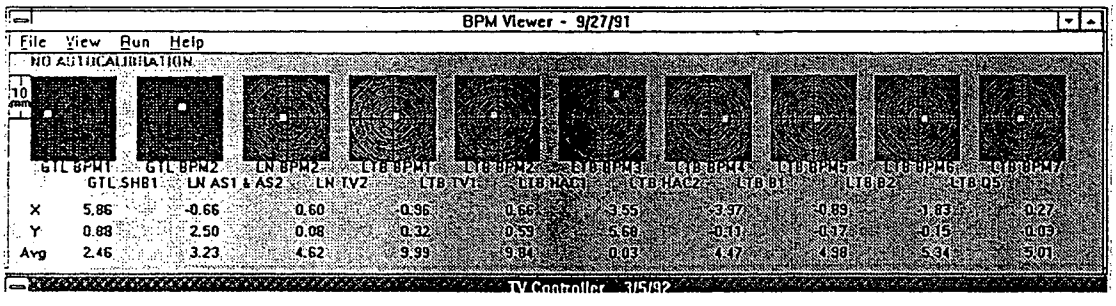

Figure 17. A display of measured beam positions in the linac and LTB line. LTB BPM3 is not in the beam passage.

When storage ring or booster beam is measured, the peak-detector output is essentially DC when the beam orbits continuously. In this case the S-H is used as an impedance buffer and simply tracks the input voltage. The low-pass filter (1 kHz) following the S-H removes high frequency noise from the signal before it is digitized. This information was used to calculate the necessary strength of the booster trim magnets to correct the closed-orbit distortions.[9] Storage ring orbit corrections and real-time orbit stabilization will also utilize this signal. Correcting and stabilizing the closed orbit in the storage ring is more important because of the small dynamic aperture beam line requirements.

In the third signal processing branch the BPM video signal is again peak-detected and digitized by a fast 8-bit analog-to-digital converter (FAD) which enables the BPM to make single-turn position measurements. This single turn capability makes the ALS BPM system unique. There are two FAD modules in the storage ring and booster ring BPM bins. The function of these modules is to capture a time record of turn-by-turn beam position data for later analysis. The video input of the FAD drives a fast peak detector having a MOS-FET reset switch. The peak detector output buffer amplifier drives the input of an 8-bit flash A/D. The A/D captures the voltage peak (2V maximum) and drives two first-in-first-out (FIFO) memory chips via an 8-bit buss.

The timing of a FAD sequence is as follows: The ILC sets up FAD operation by clearing any old FIFO data and rearming trigger circuitry. Slightly before beam signals appear at the ring orbit frequency, the reset FET is gated on and the storage capacitor discharged. The FET drive pulse ends and the beam signal appears at the input of the peak detector. Just before the next ring orbit clock pulse arrives the A/D is triggered to acquire the peak of the detected beam signal. After A/D acquisition the FIFOs are strobed to store the data. One FIFO in each channel takes data at the ring orbit frequency. Another FIFO takes data at f_0, $f_0/10$, $f_0/100$, or $f_0/1000$, the rate being set in advance by the ILC via the Timing/Calibration module. This operation continues until an a-synchronous "Halt" pulse (derived in external circuitry) arrives at the bin promptly stopping signal acquisition. All BPM bins receive the "Halt" pulse at the same time. The ILC detects the halted condition and reads the contents of the FIFO memory. Input/output operation of the FIFOs is controlled by a programmable array logic (PAL) chip via commands from the ILC.

Figure 18 shows a typical FAD data. [10] The first two traces on the top in figure 18 show the horizontal and vertical beam positions for the 1024 consecutive turns (250 nsec) starting from 0.5 msec after the injection. This information was calculated from the fast FIFO beam orbit data. The slow FIFO may have a time record up to 250 ms long (albeit with 999 out of 1000 beam signals missing). The vertical and horizontal booster tunes were calculated by fast-Fourier-transformation of the first two traces and the results are displayed in figure 18. The measured booster tunes agree very well with our tune model based on the magnet measurements. [11] The fast FIFO data were also used to calculate beam positions in the first few turns. This type of data processing requires careful calibration of the BPM electronics.

6.5 BPM Calibration and timing

The calibration and timing module provides timing pulses for the IF and FAD modules. In addition, it generates calibration signals which are used to measure relative gain in the four channels. Input and output operations of the module are controlled by the ILC via a PAL chip. The calibrator is used to measure differential gain in the RF, IF, and ILC modules. A calibration sequence goes as follows: After the gain of the IF amplifiers has been set by the ILC and beam signals have been acquired, the GaAs switches in the RF module are switched to the calibration input. The calibrator is off at this time as a sample of no-signal offsets is measured. The beam signals are terminated in 50 ohms in the switches. Switch isolation at 500 MHz is about 50 dB. The calibrator is turned on, and the calibration signal level is automatically adjusted to equal the maximum detected beam signal. The difference between detected calibration signals is measured and gain-offset coefficients calculated. During subsequent beam measurements the measured offsets are subtracted from beam signals and gain coefficients applied to scale the raw beam signal data. With this method we have demonstrated in a bench test 0.03 mm repeatability over a 40 dB range of RF test signals. When the BPM measures multi-bunch beam the calibrator pulse length is set to 500 ns. Single bunch beam is

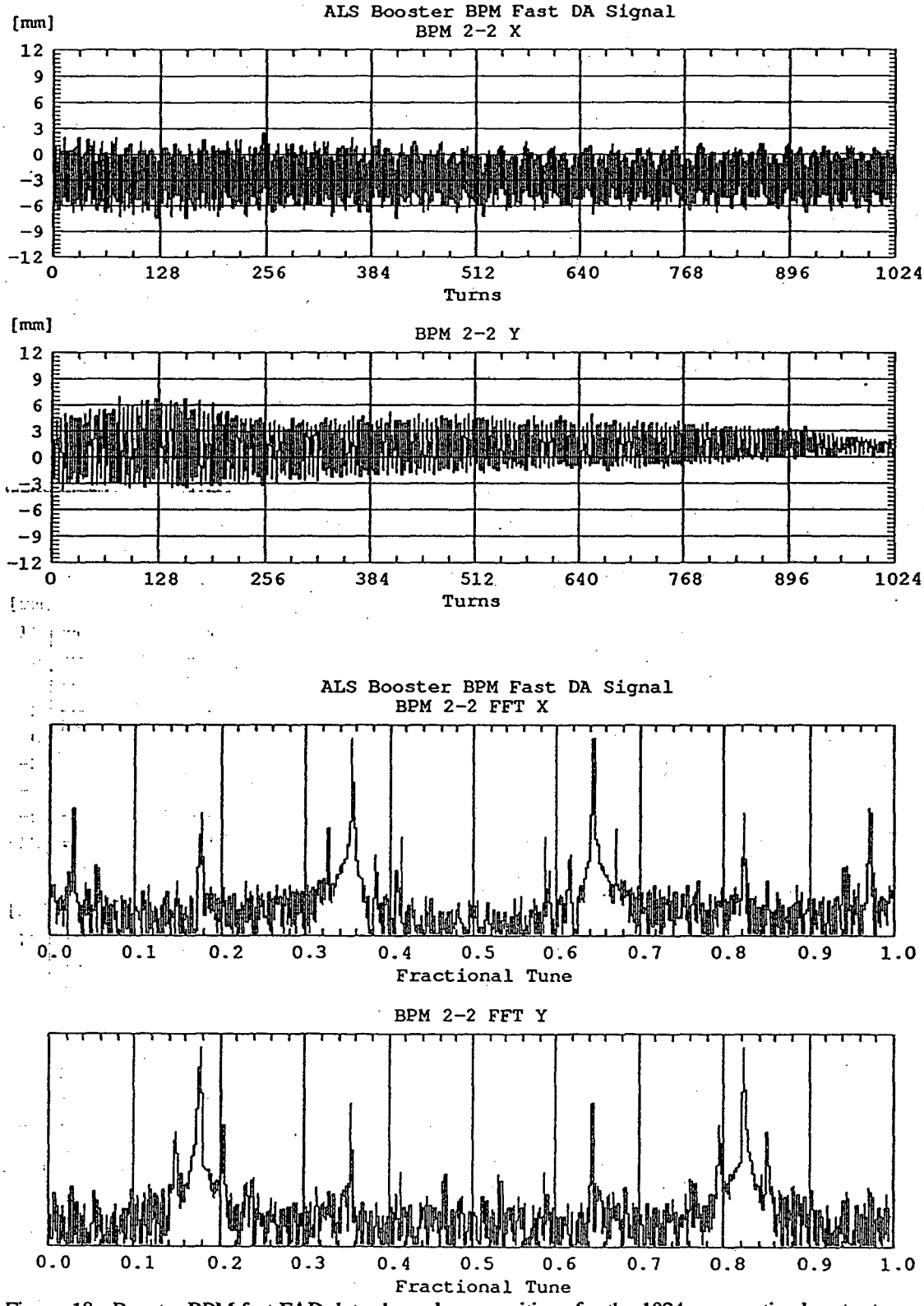

Figure 18. Booster BPM fast FAD data shows beam positions for the 1024 consecutive booster turns (250 nsec) 500 microseconds after injection.

simulated by a 75 ns calibration signal. This helps compensate slightly different transient response in the BPM amplifiers.

7. Conclusion

The accelerator instrumentation played the roles of our ears and eyes in commissioning and operating the ALS injector accelerator. We had adequate accelerator instrumentation in most of the accelerator. The cost of the instrumentation is small compared with other costs and was well worth it for saved time and efforts during commissioning. We felt that we could have used more diagnostics such as BPMs and steering magnets in the GTL line. More diagnostics at the linac exit such as total charge monitors and fast speed diagnostics are becoming commercially available. This will make commissioning more enjoyable.

The BPMs were indispensable part of our instrumentation, but we have learned a lot during our commissioning how to use them and interpret the data properly.

Acknowledgments

Authors wish to thank all the ALS accelerator systems group for their long time of hard work which produced the data presented in this paper. Special thanks go to Alan Jackson, Rodich Keller, Dexter Massoletti, and Hiroshi Nishimura for valuable discussions, suggestions and encouragement. Many thanks are also due to the ALS engineering staff built the accelerator and made all the hardware and software running. This work was supported by the Director, Office of Energy Research, Office of Basic Energy Sciences, Materials Sciences Division of the U.S. Department of Energy, under Contract No. DE-AC03-76SF00098.

References

[1] "1-2 GeV Synchrotron Radiation Source Conceptual Design Report," LBL Report PUB-5172Rev, July 1986

[2] "The Advanced Light Source - Status Report," A. Jackson, Proceedings of the 1991 IEEE Particle Accelerator Conference, San Fransisco, page 2637 (1991)

[3] "Injection System Design for the LBL 1-2 GeV Synchrotron Radiation Source," F. Selph, A. Jackson, and M.S. Zisman, Proceedings of the 1987 IEEE Particle Accelerator Conference, Washington, D.C., page 446 (1987)

[4] "Commissioning Experiences of the ALS Booster Synchrotron," C. Kim, Proceedings of the 1991 IEEE Particle Accelerator Conference, San Fransisco, page 2691 (1991)

[5] "Design of a Bunching System for a High Intensity Electron Linac," R. Miller, C. H. Kim, and F. Selph, Proceedings of the European Particle Accelerator Conference, Rome, page 863 (1988)

[6] "Advanced Light Source Beam Position Monitor," J. Hinkson, Proceedings of the 1991 CEBAF Accelerator Instrumentation Workshop

[7] K. Halbach, "Description of Beam Position Monitor Signals with Harmonic Functions and their Taylor Series Expansions," Lawrence Berkeley Laboratory AFRD Report, LBL22840

[8] S. Magyary, et al., "Advanced Light Source Control System," in Proceedings of IEEE Particle Accelerator Conference, Vol. 1, p. 74, (1989)

[9] Lindsay Schachinger, private communications

[10] Courtesy of Hiroshi Nishimura

[11] "Magnet Data Analysis for the ALS Lattice Magnets," R. Keller, Proceedings of the 1991 IEEE Particle Accelerator Conference, San Fransisco, page 2113 (1991)

LAWRENCE BERKELEY LABORATORY
UNIVERSITY OF CALIFORNIA
TECHNICAL INFORMATION DEPARTMENT
BERKELEY, CALIFORNIA 94720